Photophoretic manipulation of absorbing aerosol particles with vortex beams: theory versus experiment

Anton S. Desyatnikov[1*], Vladlen G. Shvedov[1–3], Andrei V. Rode[3], Wieslaw Krolikowski[3], and Yuri S. Kivshar[1]

[1]*Nonlinear Physics Center, Research School of Physics and Engineering, The Australian National University, Canberra ACT 0200, Australia*
[2]*Department of Physics, Taurida National University, Simferopol 95007 Crimea, Ukraine*
[3]*Laser Physics Center, Research School of Physics and Engineering, The Australian National University, Canberra ACT 0200, Australia*
asd124@rsphysse.anu.edu.au

Abstract: We develop a theoretical approach for describing the optical trapping and manipulation of carbon nanoclusters in air with a dual-vortex optical trap, as realized recently in experiment [V. Shvedov *et al.*, Opt. Express **17**, 5743 (2009)]. We calculate both longitudinal and transverse photophoretic forces acting on a spherical absorbing particle, and then compare our theoretical predictions with the experimental data.

OCIS codes: (350.4855) Optical tweezers or optical manipulation; (260.6042) Singular optics.

References and links

1. K. Dholakia, P. Reece, and M. Gu, "Optical micromanipulation," Chem. Soc. Rev. **37**, 42-55 (2008).
2. A. Ashkin, "Acceleration and trapping of particles by radiation pressure," Phys. Rev. Lett. **24**, 156-159 (1970).
3. A. Ashkin, J. M. Dziedzic, J. E. Bjorkholm, and S. Chu, "Observation of a single-beam gradient force optical trap for dielectric particles," Opt. Lett. **11**, 288-290 (1986).
4. E. J. Davis and G. Schweiger, *The Airborne Microparticle: Its Physics, Chemistry, Optics, and Transport Phenomena*, (Springer, 2002), pp. 780-785.
5. F. Ehrenhaft, "On the physics of millionths of centimeters," Phys. Z. **18**, 352-368 (1917).
6. O. Preining, "Photophoresis," in *Aerosol Sciences* Ed. C. N. Davies (Academic Press, N. Y. 1966), pp. 111-135.
7. V. G. Shvedov, A. S. Desyatnikov, A. V. Rode, W. Krolikowski, and Yu. S. Kivshar, "Optical guiding of absorbing nanoclusters in air," Opt. Express **17**, 5743-5757 (2009), http://www.opticsinfobase.org/oe/abstract.cfm?URI=oe-17-7-5743
8. H. Rubinsztein-Dunlop, T. A. Nieminen, M. E. J. Friese, and N. R. Heckenberg, "Optical trapping of absorbing particles," Adv. Quant. Chem. **30**, 469-492 (1998).
9. D. McGloin, D. R. Burnham, M. D. Summers, D. Rudd, N. Dewara, and S. Anand, "Optical manipulation of airborne particles: techniques and applications," Faraday Discuss. **137**, 335-350 (2008).
10. A. V. Rode, E. G. Gamaly, and B Luther-Davies, "Formation of cluster-assembled carbon nano-foam by high-repetition-rate laser ablation," Appl. Phys. A **70**, 135-144 (2000).
11. A. V. Rode, R. G. Elliman, E. G. Gamaly, A. I. Veinger, A. G. Christy, S. T. Hyde, and B. Luther-Davies, "Electronic and magnetic properties of carbon nanofoam produced by high-repetition-rate laser ablation," Appl. Surf. Science **197-198**, 644-649 (2002).
12. J. F. Nye and M. V. Berry, "Dislocations in wave trains," Proc. R. Soc. London A **336**, 165 (1974).
13. M. S. Soskin and M. V. Vasnetsov, "Singular Optics," Prog. Opt. **42**, 219-276 (Ed. E. Wolf, Elsevier, 2001).
14. C. N. Alexeyev, M. A. Yavorsky, and V. G. Shvedov, "Angular momentum flux of counter-propagating paraxial beams," J. Opt. Soc. Am. B **25**, 643-646 (2008).
15. *Structured Light and its Applications: An Introduction to Phase-Structured Beams and Nanoscale Optical Forces*, ed. D. L. Andrews (Elsevier, Academic Press, 2008).
16. G. T. Best and T. N. L. Patterson, "The capture of small absorbing particles by the solar radiation field," Planet. Space Sci. **9**, 801-809 (1962).

#109734 - $15.00 USD Received 6 Apr 2009; revised 27 Apr 2009; accepted 27 Apr 2009; published 30 Apr 2009

17. G. M. Hidy and J. R. Broc, "Photophoresis and the descent of particles into the lower stratosphere," J. Geophys. Res. **72**, 455 (1967).
18. A. A. Cheremisin, Yu. V. Vassilyev, and H. Horvath, "Gravito-photophoresis and aerosol stratification in the atmosphere," J. Aerosol Sci. **36**, 1277-1299 (2005).
19. G. Wurm and O. Krauss, "Experiments on negative photophoresis and application to the atmosphere," Atm. Env. **42**, 2682-2690 (2008).
20. O. Krauss, G. Wurm, O. Mousis, J.-M. Petit, J. Horner, and Y. Alibert, "The photophoretic sweeping of dust in transient protoplanetary disks," Astron. Astrophys. **462**, 977 (2007).
21. O. Mousis, J.-M. Petit, G. Wurm, O. Krauss, Y. Alibert, and J. Horner, "Photophoresis as a source of hot minerals in comets," Astron. Astrophys. **466**, L9-L12 (2007).
22. L. D. Reed, "Low Knudsen number photophoresis", J. Aerosol Sci. **8**, 123-131 (1977).
23. J. C. Maxwell, "On Stresses in Rarified Gases Arising from Inequalities of Temperature," Phil Trans. R. Soc. London **170**, 231-256 (1879).
24. S. Beresnev, V. Chernyak, and G. Fomyagin, "Photophoresis of a spherical particle in rarefied gas," Phys. Fluids A **5**, 2043-2052 (1993).
25. Yu. I. Yalamov, V. B. Kutukov, and E. R. Shchukin, "Theory of the photophoretic motion of the large-size volatile aerosol particle," J. Colloid Interface Sci. **57**, 564 (1976).
26. S. Arnold and M. Lewittes, "Size dependence of the photophoretic force", J. Appl. Phys. **53**, 5314 (1982).
27. P. W. Dusel, M. Kerker, and D. D. Cooke, "Distribution of absorption centers within irradiated spheres", J. Opt. Soc. Am. **69**, 55 (1979).
28. Yu. I. Yalamov, V. B. Kutukov, and E. R. Shchukin, "Motion of a small aerosol particle in a light field," J. Eng. Phys. **30**, 648-652 (1976).
29. M. Kerker and D. D. Cooke, "Photophoretic force on aerosol particles in the free-molecule regime", J. Opt. Soc. Am. **72**, 1267 (1982).
30. M. Lewittes, S. Arnold, and G. Oster, "Radiometric levitation of micron sized spheres," Appl. Phys. Lett. **40**, 455 (1982).

1. Introduction

Micromanipulation of particles with laser light [1] was pioneered by A. Ashkin almost 40 years ago [2], and it was developed further shaping into a special field commonly refereed to as *optical tweezers* [3]. The operation principle of optical tweezers is based on utilization of the radiation pressure (RP) force applied by a laser beam via a transfer of the momentum from photons refracted in transparent particles (gradient force) or scattered by and absorbed in opaque particles. In the latter case, the heating of absorbing particles by light may lead to dominating thermal forces [4], such as the *photophoretic* (PP) force [5, 6], which produce a detrimental effect preventing the use of the RP-based optical tweezers [2]. However, we have demonstrated recently in experiment that the photophoretic forces acting on strongly absorbing ('black') particles in open air can be tailored in such a way that they allow trapping and manipulation of clusters of carbon nanoparticles [7].

In contrast to absorbing colloids [8] or transparent aerosols [9], the photophoretic force always dominates for absorbing aerosols. Using the available theory for spherical particles illuminated by a plane wave, we have estimated earlier [7] that the photophoretic force can become 10^4 times stronger than the RP force for the particles made of carbon nanofoam [10, 11]. However, the PP trap should be created with optical vortex beams [12, 13], and it has a spatially varying 'doughnut-like' transverse intensity profile with a node at the origin [7]. Therefore, although the full treatment of the PP trapping problem is beyond the scope of this work, here we attempt to calculate the PP forces induced by counter-propagating vortex beams similar to the experimental geometry adopted in Ref. [14]. In particular, we show that the fraction of the optical-vortex power absorbed by a particle and both PP and RP forces are two orders of magnitude lower than that originated from a plane wave. Furthermore, to characterize the on-axis guiding of particles observed experimentally [7], we introduce a simple theoretical model which allows one to perform straightforward calculations of the trapping position, being in a good correspondence with the experimental data.

The theory of optical tweezers is well developed (see, e.g., some references in Refs. [1, 7]),

#109734 - $15.00 USD Received 6 Apr 2009; revised 27 Apr 2009; accepted 27 Apr 2009; published 30 Apr 2009

including the use of optical vortex beams [8, 15]. At the same time, the theory of photophoretic forces was developed mainly in applications to aerosol [6, 4], atmospheric [16, 17, 18, 19], and planetary [20, 21] sciences, instead of the optical trapping. Our approach [7] is based on the theory developed for micron-sized spherical particles in air, for which the Knudsen number is small (the key parameter of PP [22]), $K = l/a = 0.065$, here $l = 65$ nm is the mean-free path of air molecules and the particle-sphere radius $a = 1\,\mu$m. The PP force is a result of the Maxwellian "thermal creep" of gas molecules along a temperature gradient on the particle surface [23] and the gas is modeled as a continuous fluid medium with boundary slip flow conditions. We use [7] the expression for PP force derived in Ref. [24] (formula (34)) in the limit $K \to 0$, but similar results were also obtained by other authors [22, 25, 26],

$$F_{pp} = -J_1 \frac{9\pi\mu_a^2 aI}{2\rho_a T(k_f + 2k_a)}, \tag{1}$$

here I is the illuminating (plane wave) intensity, the gas viscosity μ_a, mass density ρ_a, average temperature T, and k_a and k_f are the thermal conductivities of gas and the particle, respectively.

It is instructive to note that the magnitude and direction of the photophoretic force greatly depend on the size of the individual particle. Since the temperature distribution on the particle surface determines the PP force, it was suggested that the "source function" proportional to the internal intensity [27] must be a key factor. In other terms, the PP force (and its direction) depends on the measure J_1 of the asymmetry of the internal heat sources [26], the later is defined as a weighted integral over normalized internal intensity [25]. The calculations of the internal field suggested, e.g., that intensity and thus the temperature of subwavelength carbon particles with $0.5 < \alpha < 2$ (here $\alpha = 2\pi a/\lambda$ is the size parameter) will be higher on the back-side from the plane wave illumination and the PP force will thus be negative (towards the source), while for $2 \leq \alpha \leq 5$ is almost symmetric and thus the PP force must be close to zero.

The same method of calculation of the internal source function of the particle with complex refractive index was also used [28, 29] in the so-called free molecules regime, for $K > 1$, where the gas kinetic theory applies instead of Eq. (1). It was found that, while for small α the PP force is positive, there is a critical value of α where the PP force changes its sign. The critical (turning) value of α can be used to recover the imaginary part and the extinction coefficient of the complex refractive index. For carbon the turning point is about $\alpha \geq 0.4$ [27] while for the volatile particles (absorbing particles changing mass), e.g. the electrostatically suspended evaporating glycerol spheres [26], the turning point is measured to be $\alpha = 11.7$. The factor J_1 was found for $\alpha = 16$ to be $J_1 = -0.34$ and thus very close to the largest *black-body value* $J_1 = -0.5$.

For calculations of the J_1 factor mentioned above the Mie scattering theory for a spherical particle illuminated by a plane wave was employed. Here we attempt to overcome this limitation and take into account the spatially varying vortex intensity. In general, the solution to the electrodynamic problem with non-uniform illumination can be obtained, for spherical particles with given optical properties, as a superposition of known Mie solutions for plane waves. However, the nanoclusters [7] have random shape and they are composite of carbon nanoparticles, thus the optical properties are determined by a complex multiple scattering and can be only estimated using rough effective medium approach. Therefore, instead of involving calculations with Mie solutions here we adopt a somewhat intuitive approximate theoretical approach.

The structure of the paper is the following. The longitudinal RP and PP forces are derived in Sec. 2 and the transverse PP force in Sec. 3. In Sec. 4, the resulting formulas are applied to the calculation of the equilibrium position of a particle on axis of the dual-vortex beam trap, these results are employed in Sec. 5 for a direct comparison with experimental data reported in Ref. [7]. Section 6 concludes the paper.

#109734 - $15.00 USD Received 6 Apr 2009; revised 27 Apr 2009; accepted 27 Apr 2009; published 30 Apr 2009

2. Longitudinal forces

In this section we calculate the RP and PP forces induced on a spherical particle located on the axis of a diffracting vortex beam.

2.1. Radiation-pressure force

The estimation of the RP force $F_a = P_a/c$ exerted on a particle requires calculation of the absorbed power P_a. For a better comparison with the PP theory for a plane wave illumination we first introduce the characteristic intensity of such hypothetical plane wave, $I_0 = P/4\pi w^2$ (see Fig. 1(a)), where $P = \int I d\vec{\rho}$ is the beam power of a Laguerre-Gauss LG_{01} beam (single-charge optical vortex) with the intensity

$$I(\rho,z) = \frac{P}{\pi}\frac{\rho^2}{w^4(z)}\exp\left(-\frac{\rho^2}{w^2(z)}\right). \tag{2}$$

Here the ring radius $w(z) = w_0\sqrt{1+z^2/z_0^2}$ with the beam waist w_0, the diffraction length $z_0 = 2\pi w_0^2/\lambda$, and ρ is a polar radius in the plane transverse to the optical axis z. To calculate the absorbed power P_a we use the Beer-Lambert law for the intensity I_t transmitted through the nanofoam film of the thickness l_z, $I_t = I_{\rm in}\exp(-l_z/l_f)$, here $I_{\rm in}$ is the incident intensity and $l_f = 35\,\mu$m, see [7]. The power $P_a = \int (I_{\rm in} - I_t)d\vec{\rho}$ and for a spherical particle with the radius a we have $l_z = 2\sqrt{a^2-\rho^2}$ and $P_a = 2\pi\int_0^a I_{\rm in}\left\{1-\exp\left(-2\sqrt{a^2-\rho^2}/l_f\right)\right\}\rho d\rho$. For a plane wave $I_{\rm in} = I_0$ and

$$F_a = \frac{P_a}{c} = \frac{\pi a^2 I_0}{c}\left\{1-\frac{l_f^2}{2a^2}\,f\left(\frac{2a}{l_f}\right)\right\},\ \text{here the function } f(t) = 1-(1+t)e^{-t}. \tag{3}$$

It is important for the following to note that, for small argument $t \ll 1$, the function $f(t) \simeq t^2(1/2 - t/3)$. For the representative particle with $a = 1\,\mu$m ($2a/l_f = 0.057$) we approximate the absorbed power as $P_a \simeq 4\pi I_0 a^3/3l_f$; in terms of the vortex power P corresponding force can be expressed as

$$F_a \simeq \frac{P}{c}\frac{a^3}{3w^2 l_f},\ \text{for a plane wave } I_{\rm in} = I_0.$$

Taking typical values $P = 0.01$ W and $w \geq w_0 = 8.4\,\mu$m we obtain the RP force $F_a = 4.5\times 10^{-15}$ N. Other parameters are $I_0 = 1.1$ kW cm^{-2}, $P_a = 1.35\times 10^{-6}$ W, and the absorption efficiency $\xi = P_a/P_{\rm in} = 4a/3l_f = 0.038$, here the incoming power $P_{\rm in} = \pi a^2 I_0 = 3.54\times 10^{-5}$ W.

For a spatially varying intensity of an optical vortex $I_{\rm in} = I(\rho,z)$ (see Eq. (2)) we assume that the spherical particle with radius a is located on optical axis, as shown in Fig. 1 (a), at the distance $z = Z$ from the beam waist at $z = 0$. In our experiments $z_0 = 837.3\,\mu$m, thus we can neglect the variation of the vortex intensity on the distances $Z - a \leq z \leq Z$, comparable with the particle size $a = 1\,\mu\text{m} \lesssim w_0 \ll z_0$, taking

$$w^2(z-Z) = w_0^2\left(1+\frac{(z-Z)^2}{z_0^2}\right) \simeq w_0^2\left(1+\frac{Z^2}{z_0^2}\right) = w^2(Z). \tag{4}$$

The incoming power is given by $P_{\rm in} = P\,f\left(a^2/w^2\right)$ and, for particles smaller than the vortex ring $a \ll w$, we use the expansion of the function $f(t)$ after Eq. (3) to obtain $P_{\rm in} \simeq Pa^4/2w^4 = 10^{-6}$ W. It is a factor of $2a^2/w^2 \leq 0.028$ smaller than the corresponding power of a "plane-wave" above, $P_{\rm in} = Pa^2/4w^2$, because of the intensity zero at the vortex origin, see the red-shaded region in Fig. 1 (a). Similarly, the absorbed power is two orders of magnitude lower,

#109734 - $15.00 USD Received 6 Apr 2009; revised 27 Apr 2009; accepted 27 Apr 2009; published 30 Apr 2009

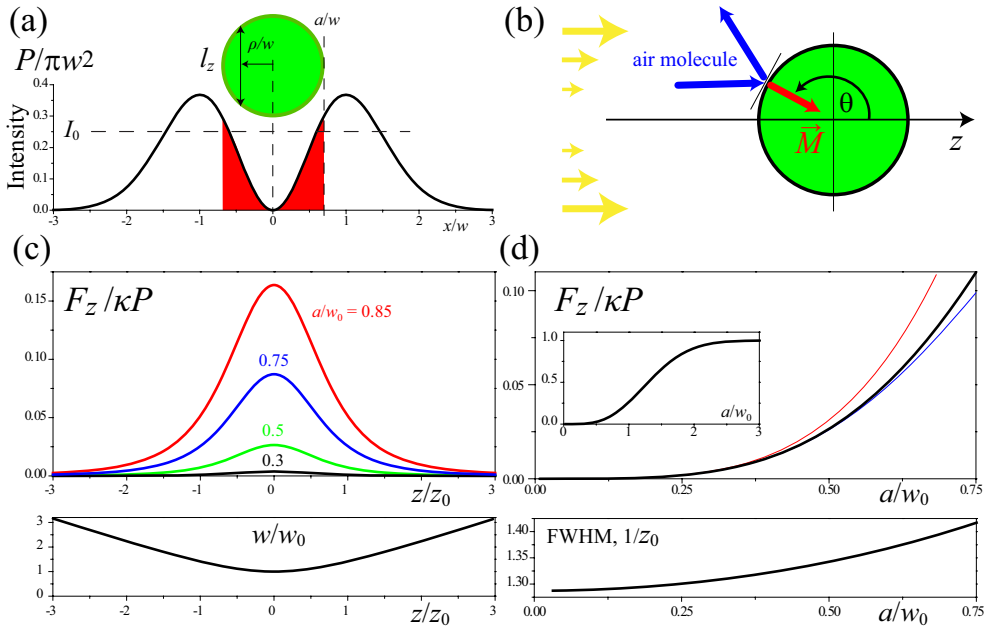

Fig. 1. Longitudinal force on a particle located on-axis of a vortex beam. (a) Vortex intensity cross-section; red-shaded is the part of a vortex beam illuminating particle (green sphere). (b) Transfer of a momentum (red arrow) from a gas molecule to a particle; the illuminated side of the particle is a hemisphere $\pi/2 \le \theta \le \pi$, θ being a polar angle. (c) The PP force Eq. (6) versus axial distance z, the bottom frame shows the ring radius $w(z)$ of the diffracting vortex beam. (d) Amplitude ($f(a^2/w_0^2)$, top) and the full width at half maximum (FWHM, bottom) of the PP force curves shown in (c). The red and blue curves in (d) show the lowest order approximations of Eq. (6): $f(t) \simeq t^2/2$ (red) as in Eq. (7), and taking into account next term $f(t) \simeq t^2(1/2 - t/3)$ (blue).

$P_a = 3.1 \times 10^{-8}$ W, than that for a plane wave above (the absorption efficiency is, of course, roughly the same $\xi = 16a/15l_f = 0.031$); to the leading order of the small parameter $a/w \ll 1$ the RP force is given by

$$F_a \simeq \frac{P}{c}\frac{8a^5}{15w^4 l_f}, \text{ for a vortex beam } I_{\text{in}} = I(\rho, Z). \tag{5}$$

It is useful to compare the obtained estimates with a gravitational force, $F_g = mg = 4.1 \times 10^{-16}$ N, as if our laser beam was used in vertical direction to levitate particle in vacuum, here $g = 9.81$ m s^{-2} is the standard gravity and the particle mass $m = 4\pi\rho_f a^3/3 = 4.2 \times 10^{-14}$ g with the characteristic mass density of the nanofoam $\rho_f = 10$ mg cm^{-3} [7]. In particular, the RP force in Eq. (5), $F_a = 10^{-16}$ N, exerted by a vortex beam with power $P = 0.01$ W is insufficient to compensate gravitational force. Note, however, that the ratio F_a/F_g scales as a^2 (limited by the assumptions above $a \ll w$ and $a \ll l_f$), so that the RP can overcome gravity for larger particles as well as for higher optical power P.

2.2. Photophoretic force

As we demonstrated above the amount of optical power absorbed by a nanocluster is very low because of a large absorption depth in nanofoam, therefore, we can neglect the distortion of

#109734 - $15.00 USD Received 6 Apr 2009; revised 27 Apr 2009; accepted 27 Apr 2009; published 30 Apr 2009

vortex beam intensity by the particle. Then, because of low thermal conductivity, we assume that the temperature changes on the particle surface are determined by the illuminating intensity I, similar to the black body particles. Finally, we introduce the area density of the linear momentum flux, $|\vec{M}| = \kappa I$, transferred from gas molecules to the particle, as shown in Fig. 1(b). The phenomenological coefficient κ has the dimension of inverse velocity and absorbs thermal and optical parameters of the gas and the particle. By definition, the PP force is given as an integral over the momentum flux density, $\vec{F} = \int \vec{M} dS$, here $dS = 2\pi a^2 \sin\theta d\theta$ is particle surface element taking into account cylindrical symmetry of the problem. The longitudinal PP force F_z is given by (see Fig. 1(b))

$$F_z = \int_{S_+} M_z dS, \quad M_z = -\kappa \cos\theta \, I(S_+), \tag{6}$$

here S_+ is illuminated hemisphere, $\pi/2 \le \theta \le \pi$. For illumination by a plane wave with characteristic intensity I_0 we obtain $F_z = \kappa \pi a^2 I_0$. Comparison with the expression for PP force Eq. (1), $F_{pp} = 3 \times 10^{-11}$ N [7], allows us to evaluate

$$\kappa = -J_1 \frac{9\mu_a^2}{2a\rho_a T(k_f + 2k_a)} \simeq \frac{3\mu_a^2}{l_f \rho_a T(k_f + 2k_a)} = 8.5 \times 10^{-7} \ \frac{\mathrm{s}}{\mathrm{m}},$$

here the last expression is obtained with $J_1 = -\xi/2 = -2a/3l_f$ [7], derived above for small particles $a \ll l_f$, the thermal conductivity of the nanofoam $k_f = 0.0266$ W m^{-1} K^{-1} and the parameters of air are: viscosity $\mu_a = 1.73 \times 10^{-5}$ N s m^{-2}, temperature $T = 298$ K, mass density $\rho_a = 1.29$ mg cm^{-3}, and thermal conductivity $k_a = 0.0262$ W m^{-1} K^{-1}. Note that the final expression for κ does not depend on particle radius and optical power, it characterizes the transfer of momentum from air molecules to the material with given properties.

For a vortex beam the intensity $I(S_+)$ in Eq. (6) is taken from Eq. (2) with the approximation Eq. (4). Integration in Eq. (6) gives

$$F_z = \kappa P \ f\left(\frac{a^2}{w^2}\right),$$

with the function $f(t)$ defined in Eq. (3). For small particles $a \ll w$ the expression can be greatly simplified,

$$F_z \simeq \kappa \frac{P}{2} \frac{a^4}{w^4}, \tag{7}$$

and it differs from the solution for plane wave illumination above, $F_z = \kappa P a^2/4w^2$, by a factor of $2a^2/w^4 \le 0.028$, exactly the same reduction as for RP force. Therefore, the actual force exerted by a vortex beam on our representative spherical nanocluster with $a = 1\,\mu$m is $F_z = 8.4 \times 10^{-13}$ N; it is 8400 times larger than corresponding RP force Eq. (5).

The PP force Eq. (6) can be measured in units of κP and it is visualized in Fig. 1(c, d). The bell-shaped curves in (c) appear because of vortex diffraction, $w(z)$, shown in the bottom panel for better comparison. As seen in (d) the amplitude of the force saturates for large particles $a > 2w_0$ so that, for the particles with $a \lesssim 0.5w_0$, the approximation Eq. (7) is sufficiently accurate while for larger particles the next term in the expansion of $f(t)$ can be taken to improve the results. The full width at half maximum (FWHM) of the curves in (c) has weak dependance on the size parameter a/w_0 as seen in the bottom panel in (d).

3. Transverse photophoretic forces

To estimate the geometry and the magnitude of PP force in transverse plane $\vec{F}_\perp$ and evaluate its trapping efficiency we adopt the same assumptions as for the calculation of the longitudinal

#109734 - $15.00 USD Received 6 Apr 2009; revised 27 Apr 2009; accepted 27 Apr 2009; published 30 Apr 2009

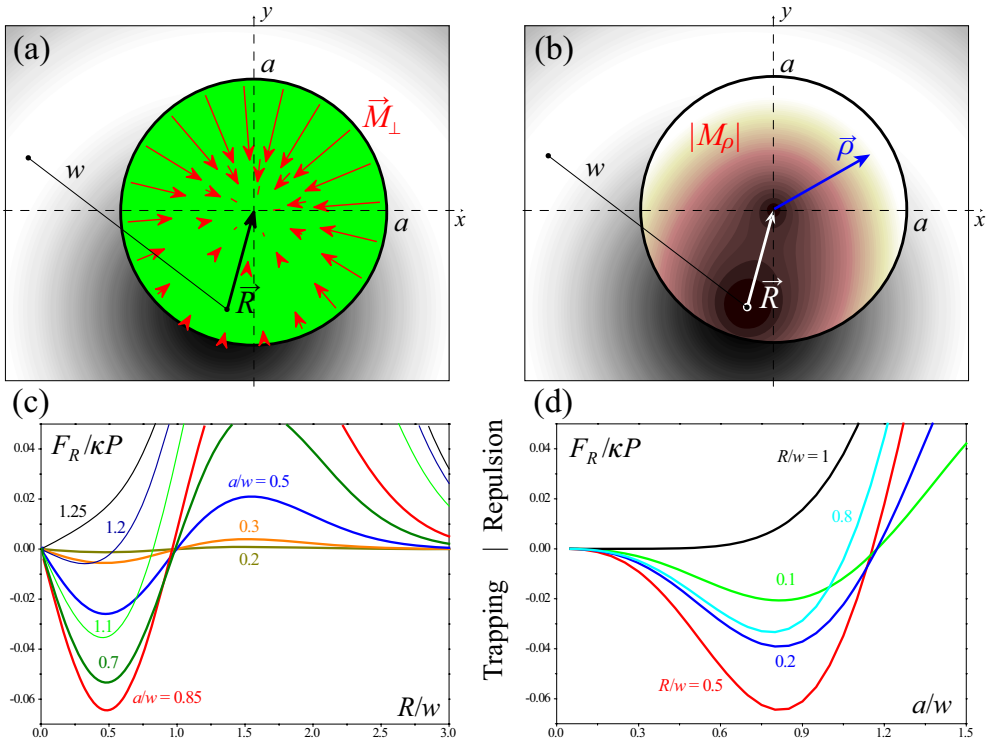

Fig. 2. Transverse photophoretic force. (a) The geometry of the problem; arrows show the transverse projection of the momentum flux density $\vec{M}_\perp$ transferred to the particle (green sphere); corresponding amplitude $|\vec{M}_\perp| = |M_\rho|$ is color-coded in (b). The background in pictures (a) and (b) is the grey-coded intensity of a vortex with the ring radius w. (c, d) The magnitude of the transverse force Eq. (8) versus two key parameters, R/w and a/w.

force above, namely we assume a spherical particle with the radius a much smaller than the diffraction length z_0 so that Eq. (4) applies. Furthermore, from the geometry of the momentum transfer depicted in Fig. 1(b) we can see that the modulus of the area density of the transverse momentum flux is given by the projection (cf. Eq. (6))

$$|\vec{M}_\perp| = \kappa \sin\theta\, I(S_+),$$

while its direction is towards the particle origin. Since $\sin\theta = \rho/a$, where ρ is the polar radius in the transverse cross-section of the particle, we derive

$$\vec{M}_\perp = -\kappa \frac{\vec{\rho}}{a} I(S_+), \quad \vec{F}_\perp \equiv \int_{S_+} \vec{M}_\perp dS = -\kappa \int_{S_+} \frac{\vec{\rho}}{a} I(S) dS.$$

We assume that the particle is shifted by a vector $\vec{R}$ from the optical axis, then the distribution of the momentum flux density is mirror-symmetric with respect to $\vec{R}$ as shown in Fig. 2(a). There are two zeros in the distribution of the amplitude $|\vec{M}_\perp|$ as seen in (b), one zero at the origin of the vortex intensity ring and another at the origin of a particle because of zero projection at $\theta = \pi$. The combination of two minima produces highly asymmetric distribution along $\vec{R}$ which is the source of the PP force returning particle to the vortex origin. It follows from the mirror symmetry that the transverse force is antiparallel $\vec{R}$ and directed towards vortex axis, $\vec{F}_\perp = \frac{\vec{R}}{R} F_R$

#109734 - $15.00 USD Received 6 Apr 2009; revised 27 Apr 2009; accepted 27 Apr 2009; published 30 Apr 2009

and $F_R \leq 0$. Therefore, for simplicity and without loss of generality we can choose, e.g., the cartesian projections $R_x = 0$ and $R_y = R$,

$$F_R = -\frac{\kappa P}{\pi} \iint_{x^2+y^2\leq a^2} \frac{y}{a} \frac{x^2+(y+R)^2}{w^4(Z)} \exp\left(-\frac{x^2+(y+R)^2}{w^2(Z)}\right) \frac{adxdy}{\sqrt{a^2-x^2-y^2}}. \qquad (8)$$

Transverse force is calculated as a function of two key parameters, R/w and a/w, the results are presented in Fig. 2(c, d). Several conclusions can be readily made. First, there is a sharp boundary between the trapping region inside the beam ($R < w$) and the repulsion of particles far from optical axis ($R > w$); the unstable equilibrium ($F_\rho = 0$) is located approximately at the ring radius $R \lesssim w$. Second, while the small particles are always trapped in the vicinity of optical axis, for particles larger than the ring $a \gtrsim w$ the trapping efficiency rapidly vanishes; the maximal trapping force is achieved for particles with $a \simeq 0.85w$. Finally, the scaling property of Eq. (8) leads to a somewhat counterintuitive result: the transverse force on a large particle ($a > 0.85w$) can grow when particle moves into the region of lower vortex intensity away from the beam focus. Indeed, the radius $w(Z)$ increases due to the diffraction and the parameter a/w decreases, thus the particle effectively follows the curves in (d) from right to left passing by the force maximum. The reason for this unexpected result, as seen in (a, b), is the interplay of geometrical contributions to the momentum flux versus spatial structure of the vortex intensity "weighting" momentum flux density in Eq. (8).

Transverse force vanishes at the vortex axis, $R \to 0$, as should be expected from symmetry considerations. Close to this equilibrium position and for small particles, $a + R \ll w_0$, we can linearize Eq. (8) and obtain

$$-F_R = \kappa P \frac{4}{3} \frac{Ra^3}{w^4(Z)} \leq \kappa P \frac{4}{3} \frac{Ra^3}{w_0^4}. \qquad (9)$$

In our horizontal scheme the transverse PP force should be compared to the gravitational force F_g (see Sec. 2 above). In particular, the equilibrium position in the transverse plane, R_0, can be found from the condition $F_g + F_R(R_0) = 0$. For our representative particle with $a = 1\,\mu$m and $F_g = 4.1 \times 10^{-16}$ N we find that the deviation from vortex center is negligible, $R_0 = 18$ nm. This estimation is supported by experimental observations [7] of trapped particles in the origin of a vortex ring. Because the PP force Eq. (9) scales as a^3, similar to F_g, it is possible to increase particle size and still balance gravitation without increasing the laser power P. In this case, however, the shift of the equilibrium position R_0 downwards from vortex axis will be stronger.

4. Equilibrium positions for the particle trapping

In this section we calculate axial positions of the PP trap determined by the balance of forces applied by forward and backward vortex beams. We study the stability of trapping position and determine its domain as a function of parameters of experimental setup.

Based on the experimental setup (see Fig. 2 in [7]) we have two principal degrees of freedom for spatial manipulation of trapped particles, apart from the total power P of the beams which defines the magnitude of the PP force. One control parameter is the distance δ between focal planes of two counter-propagating beams, adjusted by the position of the lens L4. Another is the tilt Θ of the half-wave plate WP2 defining the power ratio of two beams $\varepsilon(\Theta)$ (see Eq. 1 in [7]). Each beam applies a PP force given by Eq. (6) being a function of the position of the particle, here z, relative to the beam focal plane $z = 0$. For two beams with focuses separated by the distance δ we introduce the origin of the coordinates in the middle between focal planes located at $z = \pm\delta/2$. The total longitudinal force on the particle is then given by the sum,

#109734 - $15.00 USD Received 6 Apr 2009; revised 27 Apr 2009; accepted 27 Apr 2009; published 30 Apr 2009

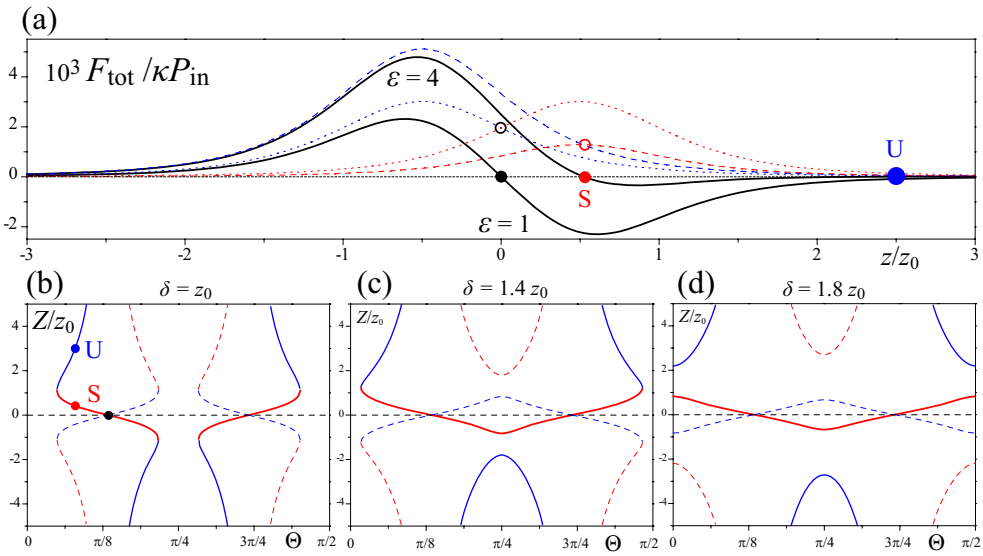

Fig. 3. Trap position. (a) The total longitudinal forces (black solid lines) for equal ($\varepsilon = 1$) and unequal ($\varepsilon = 4$) powers at the inter-focal distance $\delta = z_0$. Corresponding stable (S) and unstable (U) positions of the trap are indicated in the $Z(\Theta)$ diagram in (b). Similar diagrams (c) and (d) show stable (red) and unstable (blue) roots $Z(\Theta)$ for different values of δ: solid lines for $\delta > 0$ and dashed lines for $\delta < 0$.

$F_{\rm tot} = F_z\left(z-\delta/2; P_f\right) - F_z\left(z+\delta/s; P_b\right)$, so that using Eq. (6) we obtain

$$\frac{F_{\rm tot}(z)}{\kappa} = P_f\, f\left(\frac{a^2/w_0^2}{1+(z+\delta/2)^2/z_0^2}\right) - P_b\, f\left(\frac{a^2/w_0^2}{1+(z-\delta/2)^2/z_0^2}\right), \tag{10}$$

here P_f and P_b are the powers of the forward and backward beams, respectively. Stationary points $z = Z$ can be found from the condition $F_{\rm tot}(Z) = 0$. As we demonstrated above, the linearized expression for the force Eq. (7) provides good approximation for the particles with $2a < w_0 \le w(z)$. In this limit the stationary point (trap position Z) does not depend on the particle radius a and it is given by the solutions to a corresponding quadratic equation

$$Z^{\pm} = \frac{\delta}{2}\frac{\varsigma+1}{\varsigma-1} \pm \sqrt{\frac{\delta^2\varsigma}{(\varsigma-1)^2} - z_0^2}, \tag{11}$$

here $\varsigma^2(\Theta) = \varepsilon(\Theta)$ (see Eq. 1 in [7]). However, the stationary point can be stable or unstable. Linearizing Eq. (10) in the vicinity of a stationary point, $z = Z + \xi$ with $|\xi| \ll |Z|$, we obtain $F_{\rm tot}(Z+\xi) \simeq \xi\ (dF_{\rm tot}/dz)\,|_{z=Z}$. Therefore, the stationary point Z is *stable* if $(dF_{\rm tot}/dz)\,|_{z=Z} < 0$ (the force is returning), and it is *unstable* otherwise. Calculation of the derivative of the total force Eq. (10) gives the following result:

$$\left(\frac{dF_{\rm tot}}{dz}\right)\Big|_{z=Z^{\pm}} = \pm\,\delta\, Z^{\pm} C, \text{ here } C\left(\delta, Z^{\pm}\right) > 0. \tag{12}$$

Therefore, there is one stable and one unstable stationary point, see Fig. 3(a), and the stability is defined by the sign of the root in Eq. (11) as well as the sign of the inter-focal distance δ. For equal powers of two beams, $P_f = P_b$ and $\varsigma = 1$ at $\Theta = \pi(0.134, 0.366, 0.634, 0.866)$ (see

#109734 - $15.00 USD Received 6 Apr 2009; revised 27 Apr 2009; accepted 27 Apr 2009; published 30 Apr 2009

parameters in Eq. 1 of Ref. [7]), the force derivative is proportional to $-\delta$, instead of Eq. (12), and the trapping position $Z = 0$ is stable only for $\delta > 0$, when focal planes of two beams are separated. The case $\delta < 0$ corresponds to the anti-separated focuses; although there are stable trapping positions, they are located outside the inter-focal region where the transverse force rapidly decreases, see Sec. 2. Furthermore, the trapping is possible (the roots in Eq. (11) are real) only if the separation of focuses δ exceeds some minimal value, $|\delta| \geq z_0|\varsigma - 1|/\sqrt{\varsigma}$. Otherwise the real roots disappear and there is no stationary trapping on axis. Similarly, if we use an ideal polarizing beam splitter BS2 in our experimental scheme, so that $\alpha = 1$ and $\beta = 0$ (see Fig. 2 and Eq. 1 in [7]), the power ratio would become unbounded $\varsigma = \tan 2\Theta/\sqrt{\gamma}$ and, for any δ, the trap position with disappear (move to infinity $Z \to \infty$) for some value of Θ. It could still be used for stationary guiding of particles, as in Fig. 5 of Ref. [7], but the dynamical bouncing of particles, as in Fig. 6 of Ref. [7], will be impossible. In contrast, for our "imperfect" beam-splitter we have bounded power ratio, $0.304 \leq \varsigma(\Theta) \leq 3.953$, and there is the stationary solution Eq. (11) for any $0 \leq \Theta \leq 2\pi$ (full turn of the input polarizer) if $\delta \geq 1.485 z_0$.

Our objective here is to find, using Eq. (11), the domain L of stable trapping along optical axis as a function of δ for the given characteristic of a beam-splitter [7]. For separated focal planes $\delta > 0$ this domain includes a middle point $Z = 0$ for equal powers and it is given by $L = Z^-(\varsigma_{\max}) - Z^+(\varsigma_{\min})$, here

(i) the inter-focal distance $\delta < 1.261 z_0$: stable trapping is limited by a finite domain of Θ, for a given δ the limits satisfy $\varsigma_{\max,\min} = 1 + \Delta/2 \pm \Delta\sqrt{1 + \Delta^2/4}$, here $\Delta = \delta/z_0$, see an example in Fig. 3(b). The domain is $L = \sqrt{\delta^2 + 4z_0^2}$ so that, for $\delta \to 0$ and $\varsigma_{\max,\min} \to 1 \pm \delta/z_0$, we formally obtain the minimal value of the domain $L \to 2z_0$. However, at the limit $\delta = 0$ and $\varsigma = 1$ the force is zero everywhere, so that close to this limit the magnitude of force is infinitesimally small. The domain growths with $\delta \to 1.261 z_0$ and $L_{\max} = 2.364 z_0$.

(ii) the inter-focal distance $1.261 < \delta/z_0 < 1.485$: here $\varsigma_{\min} = 0.304$ and $\varsigma_{\max} = 1 + \Delta^2/2 + \Delta\sqrt{1 + \Delta^2/4}$. The domain L decreases monotonically from $2.364 z_0$ to $2.015 z_0$, the trapping is continuous on a limited interval of Θ, see Fig. 3(c).

(iii) the inter-focal distance $\delta > 1.485 z_0$: trapping is continuous for $\Theta \in [0, 2\pi)$ with $\varsigma_{\min} = 0.304$ and $\varsigma_{\max} = 3.953$, see Fig. 3(d). The trapping domain, $L/z_0 = 1.7762\Delta - \sqrt{0.4534\Delta^2 - 1} - \sqrt{0.6290\Delta^2 - 1}$, first decreases to reach its minimum $L_{\min} = 1.3737 z_0$ at $\delta = 2.4351 z_0$, then diverges with increasing δ.

5. Direct comparison with experiment

In this section we apply the theoretical approach developed above to compare some of the theoretical predictions with the experimental results presented earlier in Ref. [7]. We distinguish two types of optical guiding: the *static* guiding or positioning, when each trapping position is fixed in time (for minutes or hours), and the *dynamic* guiding when the trapping position is changed continuously thus setting trapped particle in motion.

The experiments were performed for continuous trapping in the whole domain $\Theta \in [0, 2\pi)$, described above in the case *(iii)* with the corresponding roots shown in Fig. 3(d). Figure 4(a) describes the static guiding (positioning), similar to Fig. 5 of Ref. [7], where the inter-focal distance $\delta \simeq 2$ mm corresponds to the minimum value of the trapping domain $L = 1.15$ mm, slightly larger than the observed guiding over the distance ~ 1 mm. Nevertheless, the slopes of the curve in Fig. 4(a) agree well with experimental data. However, this is not the case of Fig. 4(b), where the results for *dynamical* guiding, from Fig. 6 of Ref. [7], are compared to the calculations of *stationary* trap position. Indeed, the slopes of the experimental dataset are much steeper than that of the solid theoretical curve because the slope of the curve $Z(t)$ corresponds to the particle velocity, the latter reaches values up to ~ 1 cm/s, determined by measuring

#109734 - $15.00 USD Received 6 Apr 2009; revised 27 Apr 2009; accepted 27 Apr 2009; published 30 Apr 2009

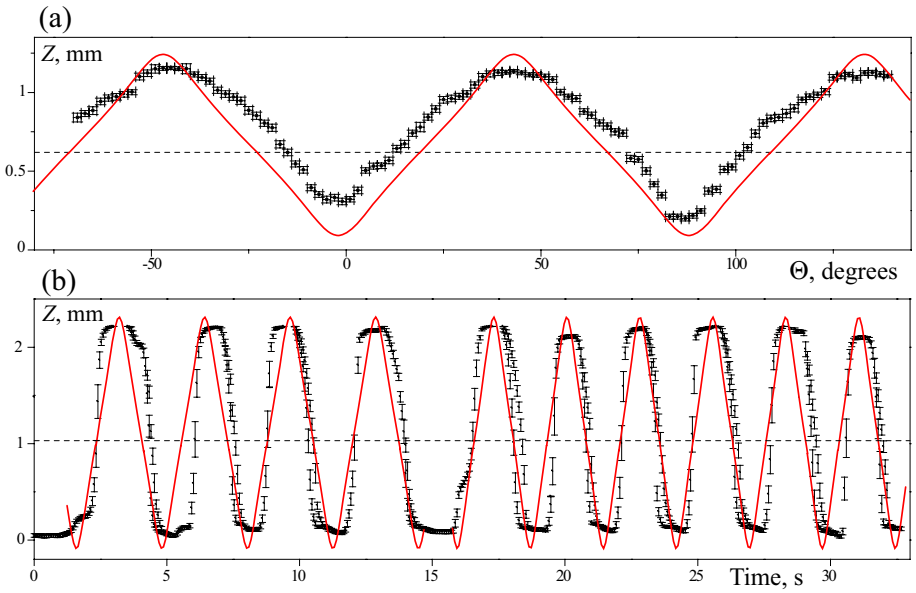

Fig. 4. Theoretically calculated position of a particle in the trap (red lines) compared with the experimental data (black bars). (a) Static guiding with each position (of the polarizer and the particle) fixed in time, as in Fig. 5 of Ref. [7]. (b) Dynamic guiding in real time with polarizer rotated and particles moving continuously, as in Fig. 6 of Ref. [7].

the longest particle tracks (vertical bars in (b)) $\sim 400\,\mu$m recorded with exposition 40 ms. Furthermore, the extrema of the experimental dataset are flatter than those of the theoretical curve, this difference is a direct manifestation of the inertia of trapped particles moving along the optical axis and spending more time close to the points of return. The discontinuity visible in the middle of the dataset in (b) is because the rotation of the half-wave plate was not monotonic. More importantly, the theoretical predictions on the trapping domain $L \simeq 2.4$ mm, calculated for the inter-focal distance $\delta \simeq 7.4$ mm used in experiment, agree well with the limits of particle motion $L_{\rm exp} \simeq 2.2$ mm recorded in experiment.

6. Conclusions

We have suggested a simple theoretical approach to describe the action of photophoretic forces on small absorbing aerosol particles. Our approach takes into account a spatially varying intensity distribution of the laser beam, and it allows us to calculate both transverse and longitudinal trapping forces as well as to determine analytically the position of a trapped particle. Our calculations show that there is an optimal size of the particle, $a = 0.85w$, with respect to the vortex radius w, for which the longitudinal and transverse forces are maximal. Further improvement of the theory presented above should include the calculation of the additional forces simultaneously acting in the trap, such as the drag forces from surrounding air for the dynamical guiding. One of the challenging problems is to describe the actual process of capturing particles passing by in the area outside the trap, the effect clearly observed in our recent experiments [7].

Acknowledgments

The authors acknowledge a support from the National Health and Medical Research Council and the Australian Research Council.

#109734 - $15.00 USD Received 6 Apr 2009; revised 27 Apr 2009; accepted 27 Apr 2009; published 30 Apr 2009